

# Evaluation of crack propagation behaviors in a T-shaped tubular joint employing tetrahedral FE modeling

Kazuhisa Yagi<sup>a,e</sup>, Satoyuki Tanaka<sup>b</sup>, Takahiro Kawahara<sup>b</sup>,  
Kanta Nihei<sup>c</sup>, Hiroshi Okada<sup>d</sup>, Naoki Osawa<sup>e</sup>

<sup>a</sup>*Sanoyas Shipbuilding Corporation,  
2767-21, Shionasu, Kojima, Kurashiki, 711-8588, Japan,  
e-mail: k-yagi@sanoyas.co.jp*

<sup>b</sup>*Graduate School of Engineering, Hiroshima University,  
4-1, Kagamiyama 1-chome, Higashi-Hiroshima, 739-8527, Japan,  
e-mail: satoyuki@hiroshima-u.ac.jp; m146691@hiroshima-u.ac.jp*

<sup>c</sup>*Kawasaki Technology Co., Ltd., 1 Kawasaki-cho 3-chome,  
Akashi, 673-0014, Japan, e-mail: nihei.kanta@khi.co.jp*

<sup>d</sup>*Department of Mechanical Engineering, Faculty of Science and Technology,  
Tokyo University of Science, 2641 Yamazaki, Noda, 278-8510, Japan,  
e-mail: hokada@rs.noda.tus.ac.jp*

<sup>e</sup>*Department of Naval Architecture and Ocean Engineering,  
Osaka University, 2-1, Yamadaoka, Suita, 565-0871, Japan,  
e-mail: osawa@naoe.eng.osaka-u.ac.jp*

---

## Abstract

Crack growth in a T-shaped tubular joint is studied using a newly developed system to simulate three-dimensional crack propagation and fatigue testing results. Tetrahedral finite element (FE) modeling is adopted to analyze a tubular structure with a curved surface crack. The virtual crack closure-integral method is used to evaluate the fracture mechanics parameters. The FE crack modeling with a remeshing procedure using an automated mesh generation system greatly simplifies the crack propagation simulation. The calculation results are compared with the experiments.

*Keywords:* Tubular joint, Fracture mechanics, Crack propagation simulation, Finite elements, Fatigue testing

---

## 1. Introduction

Steel pipes and tubular joints are commonly employed as onshore and offshore structural members in applications such as bridges, airports, rigs, and

jackets. It is imperative to examine the fatigue strength of such members to rigorously evaluate the structural integrity and reliability of the welded structural systems. Such methods for steel structures are comprehensively summarized in [1-3]. Fracture mechanics analysis and crack propagation simulation are powerful methods for evaluating fatigue strength and the behavior of crack growth. In this work, the propagation of a surface crack in a T-shaped tubular structure is studied based on a novel computational technique and experimental research.

Tubular joints are composed of a number of circular hollow sections (CHSs), and the curved surfaces of the CHS members are connected by welds. This creates a curved geometry, which results in a complex distribution of stresses around the welded joints due to welding residual stress and external loads. It is known that surface defects are sometimes found around welded joints in tubular structures and can propagate when repeatedly subjected to external loads. A surface crack around a weld may grow both circumferentially and, at the same time, toward its depth direction in the case of a curved shape. Consequently, it is possible for it to take on a doubly-curved shape [4]. With further growth, the surface crack finally becomes a through crack, penetrating the wall. To simulate the fracture behavior of a tubular joint with a curved surface crack, highly accurate modeling is required. Some research on this subject can be found in, *e.g.*, [5-10], which develop a model for curved surface crack in tubular joints to simulate crack propagation and to evaluate stress intensity factors (SIFs) using the finite element method (FEM). Although most work has used simplified models to simulate crack propagation, some has applied precise FEM modeling to simulate crack propagation with detailed weld geometry and a curved surface crack.

As computing power has increased, and costs have rapidly fallen, advanced numerical techniques for solving fracture problems in solids and structures have been developed [15-27]. Among these, tetrahedral finite element (FE) modeling has the potential to simulate the propagation of a crack with complex geometry, such as in CHS structures. In this approach, the welded tubular structures can be modeled by applying an automated tetrahedral mesh generation system based on 3D-CAD data. FE models that take into account surface defects can also be generated efficiently. So far, FE analyses of cracked welded structures and evaluations of fracture mechanics parameters have generally been carried out by using the hexahedral FEs [28-30], but methods employing tetrahedral elements have appeared [31-37]. Okada *et al.* [34] critically examined the accuracy of evaluated SIFs and concluded

that the computed fracture parameters were accurate enough even with the use of tetrahedral elements. In previous work, we have carried out fracture analyses including the simulation of crack propagation for multiple cracks [38], a circular bar [39], a cruciform welded joint [40], a T-butt joint [41] and a nuclear pressure vessel [42] as engineering applications. This modeling has sometimes required a regular arrangement of nodes along the crack front. A node-based automatic mesh generation scheme [37]-[39] can generate such FE models without any manual interventions. Therefore, the requirement of crack front mesh discretization no longer poses any problem in terms of computational cost.

In the present study, a simulation of the propagation of a surface crack in a tubular T-joint is performed using quadratic tetrahedral FE modeling and a remeshing procedure with an automated mesh generation system. An FEM pre-processing step is adopted to generate the tubular joint FE model including a surface crack, and the virtual crack closure-integral method (VCCM) for tetrahedral FEs [34] is applied to evaluate the fracture mechanics parameters. These are combined with a commercial FEM solver to simulate the crack propagation effectively. Static and cyclic loading tests of a tubular T-joint specimen are also conducted. The experimental data on the stress distribution around the welded part, surface crack trajectory, and fatigue cycles are examined by comparison of the measured and computational results. The behavior of the crack propagation is also studied.

This paper is organized as follows: Section 2 gives a brief explanation of the crack propagation simulation system. In Section 3, the results from fatigue testing a tubular T-joint are presented. In Section 4, the stress analysis and crack propagation simulations with FE modeling are described, and a discussion follows comparing the experimental with the numerical results. Section 5 summarizes.

## 2. Crack propagation simulation system

### 2.1. Procedures for the crack propagation simulation

We adopted the pre-processing software TSV-Pre [43] to simulate the crack propagation in a tubular structure. A flowchart of the simulation is shown in Fig.1. A manual operation was carried out for the FE modeling and the first step of the computation, and the subsequent calculation steps were performed automatically.

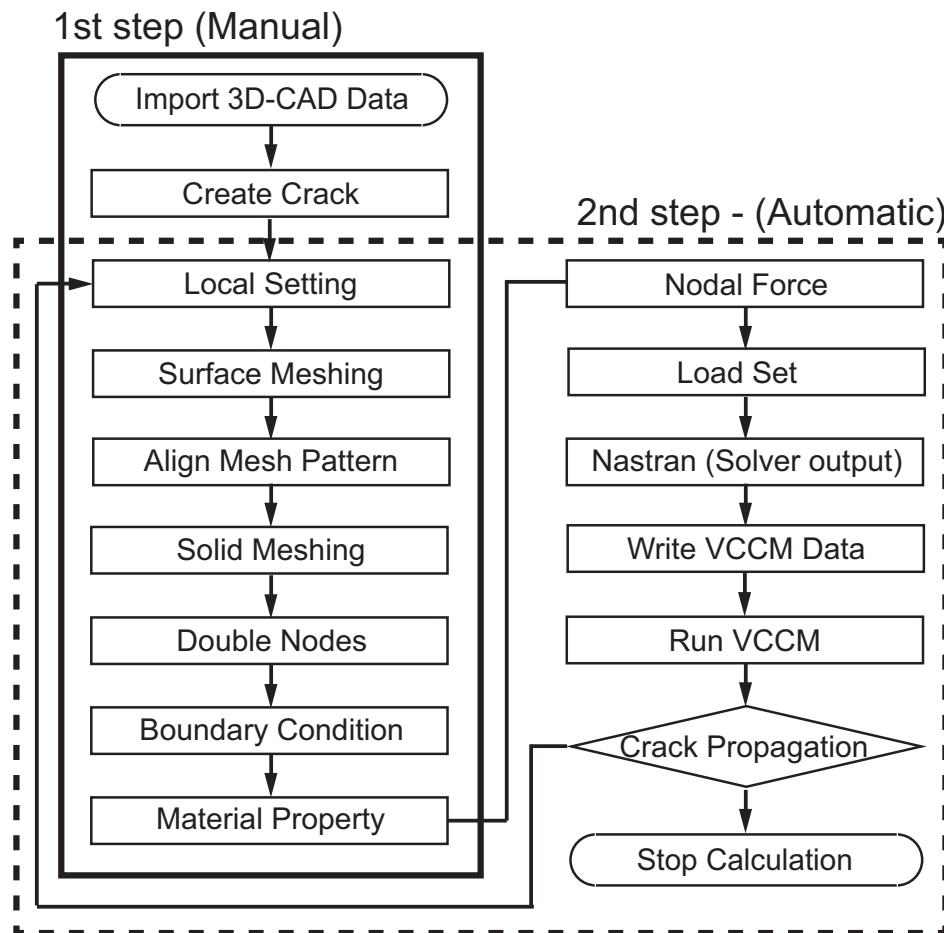


**Fig. 1.** Flowchart of the crack propagation simulation system.



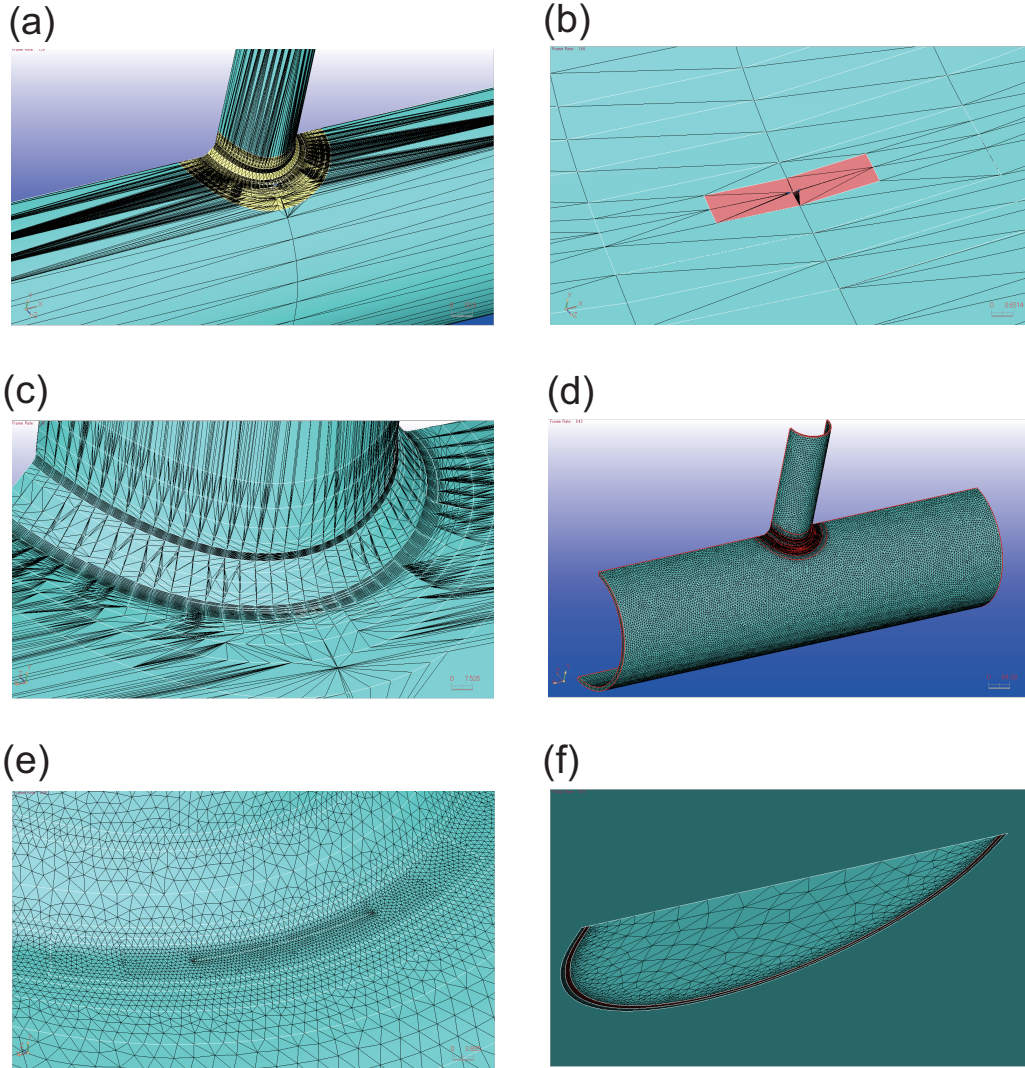


**Fig. 2.** Surface crack modeling in a tubular structure: (a) Import 3D-CAD data, (b) Create a surface crack, (c) Local parameter setting, (d) 3D FE model generation, (e) FE meshing of the weld part, (f) A surface crack embedded in the weld part.

An FE modeling of an initial crack in a T-shaped tubular joint is illustrated in Fig.2. A curved surface crack was generated as follows: An intact tubular joint was created using 3D-CAD. The CAD model was imported, and the facet data were transferred into the pre-processing software as shown in Fig.2a. An initial surface crack was inserted at the weld toe in the facet data (Fig.2b); a semi-elliptical shape was assumed. The local parameters of the FE meshing were set to accurately model the weld geometries and the surface crack with a very fine mesh. The modified CAD model around the intersection of the CHS members is presented in Fig.2c. A solid meshing with quadratic tetrahedral FEs was automatically generated in the CAD model. After this, double nodes were created on the crack face. The FE model is shown in Fig.2d. A close-up view of the welded part with a surface crack is presented in Fig.2e, and the surface crack mesh is shown in Fig.2f. A very fine structured mesh was employed to model the crack front for evaluating the SIFs.

After setting the boundary conditions and material properties, a batch process was run to run the simulation. Linear elastic analysis was used to evaluate fracture mechanics parameters of the crack. The pre-processing was combined with the commercial FEM software MSC.NASTRAN [44] on a Windows operating system. The SIFs were evaluated using the VCCM as based on quadratic tetrahedral FEs [34] in post-processing. The growth rate and direction of the surface crack were determined based on the SIFs. The details of the fracture criteria are discussed below. The surface crack geometry was updated for the calculation at each step. The remeshing procedure with automatic mesh generation was performed for the tubular structure including the extended surface crack. This batch process was iterated, and the analysis was continued until the crack reached a critical length.

## 2.2. Computation of the SIFs and the crack growth law

Mode-I, -II and -III SIFs ( $K_I$ ,  $K_{II}$  and  $K_{III}$ ) were calculated at every node along the crack front, employing the VCCM for quadratic tetrahedral FEs [34]. A surface crack embedded in an elastic body is shown in Fig.3a, where a close-up view of the crack front is also presented. The FEs were arranged equidistantly in the vicinity of the crack front to evaluate the SIFs with VCCM. The technique for extending the front's geometry is schematically illustrated in Fig.3b. The shaded region is a surface crack at cycle  $N_k$ . The nodes along the crack front are  $M_i$  ( $i=1, \dots, m$ ). The crack growth rate  $\Delta_i$  and direction  $\theta_i$  were calculated at each node based on the SIFs, and

the crack was extended for the next step. When developing the crack from cycle  $N_k$  to cycle  $N_{k+1}$ , the nodes move independently, but keeping the same number of nodes along the crack front. The curved geometry is easy to model using this approach.

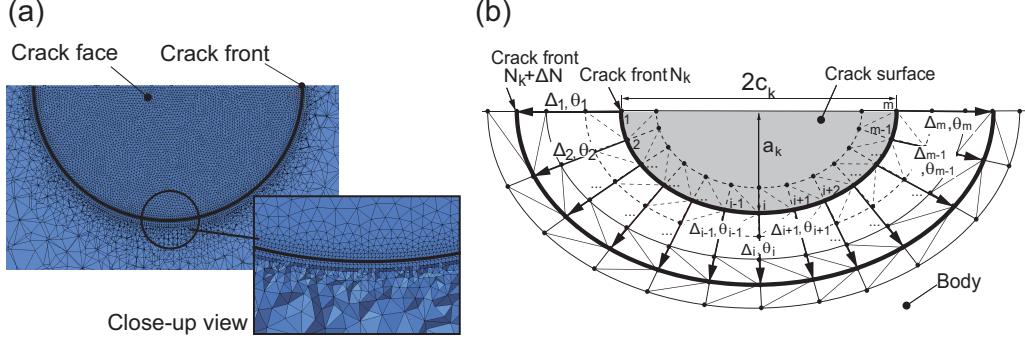


**Fig. 3.** Cross-section of a surface crack in the crack propagation system and the crack path prediction: (a) FE surface crack model, (b) A technique to extend the surface crack in the FE model.

In the VCCM computation, the SIFs are evaluated by employing the crack-opening displacements and nodal forces on the ligament as

$$K_I = \sqrt{E'G_I}, \quad (1)$$

$$K_{II} = \frac{G_{II}}{|G_{II}|} \sqrt{E'|G_{II}|}, \quad (2)$$

$$K_{III} = \frac{G_{III}}{|G_{III}|} \sqrt{2\mu|G_{III}|}, \quad (3)$$

where  $G_I$ ,  $G_{II}$  and  $G_{III}$  are the energy release rates obtained from the VCCM calculations.  $E'$  is a material parameter.  $E' = E/(1 - \nu^2)$  for the plane strain condition and  $E' = E$  for plane stress.  $E$  is Young's modulus,  $\nu$  is Poisson's ratio and  $\mu$  is the shear modulus. Although a plane stress condition is commonly assumed at the crack front location at the free surface, here a plane strain condition is employed in all the crack front nodes. Because the stress singularity at the surface point of the crack front and in its vicinity is not of the square-root type, the SIFs cannot be defined [45], and because of

the change of SIFs from the interior to the surface point, the SIF values sometimes drop abruptly at the surface point as discussed in Li *et al.* [46]. Therefore, the SIFs are extrapolated to the surface point and employed to evaluate the crack growth rate and direction. The details of the VCCM are given in [34].

It is known that fatigue cracks are generated at weld parts and grows under cyclic loadings in a welded structure. For 3D simulation of the propagation of such cracks, fracture criteria are needed to update the crack geometry, *i.e.*, prediction of the crack growth rate and direction. Several criteria have been proposed for simulating 3D mixed-mode crack propagation [47-51]. These have been determined based on Paris' law [52] and Dell'Erba and Aliabadi [48], which are tractable and easy to implement in a crack propagation simulation system. The criteria are briefly addressed below.

A periodic loading is enforced on a structure including the defects, and the SIF ranges are denoted  $\Delta K_I$ ,  $\Delta K_{II}$  and  $\Delta K_{III}$ , respectively. When Paris' law is adopted to evaluate the crack growth rate,

$$\begin{aligned}\frac{da}{dN} &= C\Delta K_{eq}^m, & \Delta K_{eq} > \Delta K_{th}, \\ \frac{da}{dN} &= 0, & \Delta K_{eq} < \Delta K_{th}.\end{aligned}\tag{4}$$

If a modified Paris' law is employed including a threshold SIF range  $\Delta K_{th}$ ,

$$\begin{aligned}\frac{da}{dN} &= C(\Delta K_{eq}^m - \Delta K_{th}^m), & \Delta K_{eq} > \Delta K_{th}, \\ \frac{da}{dN} &= 0, & \Delta K_{eq} < \Delta K_{th},\end{aligned}\tag{5}$$

where  $da/dN$  is the crack growth rate, *i.e.*, the change in crack size with respect to the number of load cycles.  $C$  and  $m$  are constants that depend on the material, load frequency, environments and mean loads.  $\Delta K_{eq}$  is a range of equivalent SIF considering the effect of the mixed mode SIFs, given by

$$\Delta K_{eq}^2 = (\Delta K_I + B|\Delta K_{III}|)^2 + 2\Delta K_{II}^2,\tag{6}$$

where  $B$  is an empirically determined factor.

To predict the direction of crack growth, a polar coordinate system is defined at the crack front, as shown in Fig.4. Here  $(n, b, t)$  are the local polar coordinates at point P, and  $(r, \theta)$  are the distance and angle in the  $n$ - $b$  plane.

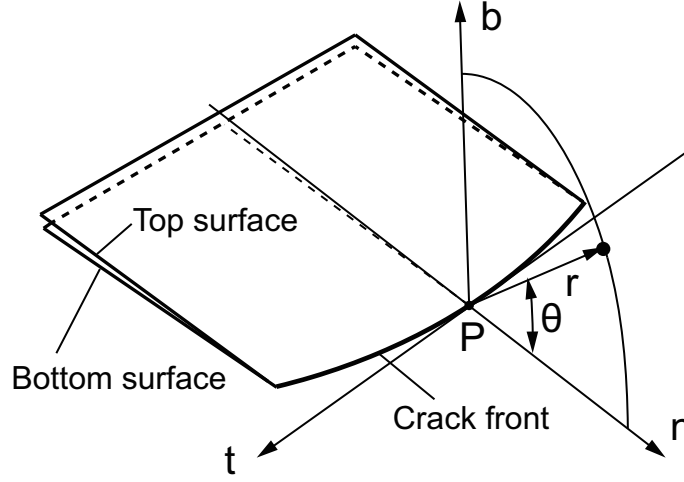


**Fig. 4.** Polar coordinates at point P along the crack front.

A maximum tangential stress criterion [53] is adopted, and the equation is written as

$$\theta = 2 \tan^{-1} \left[ \frac{-2\Delta K_{II}}{\Delta K_{Ieq} + \sqrt{(\Delta K_{Ieq})^2 + 8(\Delta K_{II})^2}} \right], \quad (7)$$

where  $\Delta K_{Ieq}$  is an equivalent SIF range including the mode-III effect. It is represented as

$$\Delta K_{Ieq} = \Delta K_I + B|\Delta K_{III}|. \quad (8)$$

The value  $B=1.0$  was adopted in Eqs.(6) and (8) (see [48]). The crack growth rate and direction were evaluated at every node along the crack front. The increments of the  $\Delta_i$  and fatigue cycles  $N$  were fixed to predict the position of the crack front in the next step. The surface crack geometry was then updated.

### 3. Fatigue testing of a tubular T-joint

Fatigue testing of a tubular T-joint was conducted to examine the crack propagation experimentally [54-56]. Four test specimens were employed, with curvature radii of the chord weld toe  $\rho=3, 6, 11$  and  $16$  mm. The radius used in this paper is  $\rho=11$  mm. An overall view of this specimen is presented

in Fig.5. The joint was composed of a brace and a chord, and the brace-chord intersection was connected by a weld. The outer diameter of the chord was 406.4 mm and the wall was 12.7 mm thick, while the outer diameter of the brace was 139.7 mm and the wall was 5.0 mm thick. A picture of the test specimen is presented in Fig.6a. The steel specification of the tubular specimen was AS1163. The chemical composition and mechanical properties are presented in Tables 1 and 2 respectively.

Table 1: Chemical analysis of the steel material.

%C	%Mn	%P	%S	%Cr	%Nb	%Cu	%Mo	%Ni	%Si	%Ti	%V	%Al	%Sn	%B	CE(IIW)	CE(Pcm)
.086	0.630	.010	.003	.017	.021	.017	.002	.020	.140	.011	<.003	.033	<.002	<.0003	.19	.12
CE Carbon Equivalent; if %C > 0.12 CE(IIW) = C + Mn/6 + (Cr + Mo + V)/5 + (Ni + Cu)/15																
CE Carbon Equivalent; if %C ≤ 0.12 CE(Pcm) = C + Si/30 + (Mn + Cu + Cr)/20 + Ni/60 + Mo/15 + V/10 + 5B																

Table 2: Mechanical properties.

Test Freq	Test Sample	Heat Treatment	Yield Strength (MPa)	Tensile Strength (MPa)	%Elongation	%Elongation $L_0 = 5.65\sqrt{S_0}$	Absorbed Energy (J)	Shear Area %
H	ChL	A					387	100
H&B	LT	A	410	500	34	32		
$L_0$ -Gauge Length; $S_0$ -Original Cross-sectional Area; H-Heat; B-Batch; A-Aged								
LT-Longitudinal Tensile; ChL-Longitudinal Charpy Impact Test								

Nine-pass, fully penetrated FCAW welding was carried out around the brace-chord intersection. The heat input of each pass ranged from 0.4 to 1.9 KJ/mm, and an E71T-1M H8 ( $\phi=1.2$ ) electrode conforming to AWS A5.20 was used. There was no heat treatment after welding. The weld toe was ground and trimmed smoothly. A surface defect was found in the fatigue testing at the saddle location on the south part of the specimen as shown in Fig.5. The weld toe geometry at the saddle location is presented in Fig.6b. The toe geometry was cast using a silicone impression material. Because the weld was ground, the weld toe cannot be clearly defined. A position "A" was therefore defined as the radiused weld toe, which is the intersection of the curvature radius and the chord surface at the saddle location.

The experimental setup is presented in Fig.7a. Both ends of the chord were supported by a pin, and uniaxial tensile loading was employed at the top of the brace. Nondestructive testing was performed before the experiments, and no major defects were found in the weld. A preliminary static load test was conducted, in which a total of  $P_{static}=70$  KN was applied to the top of



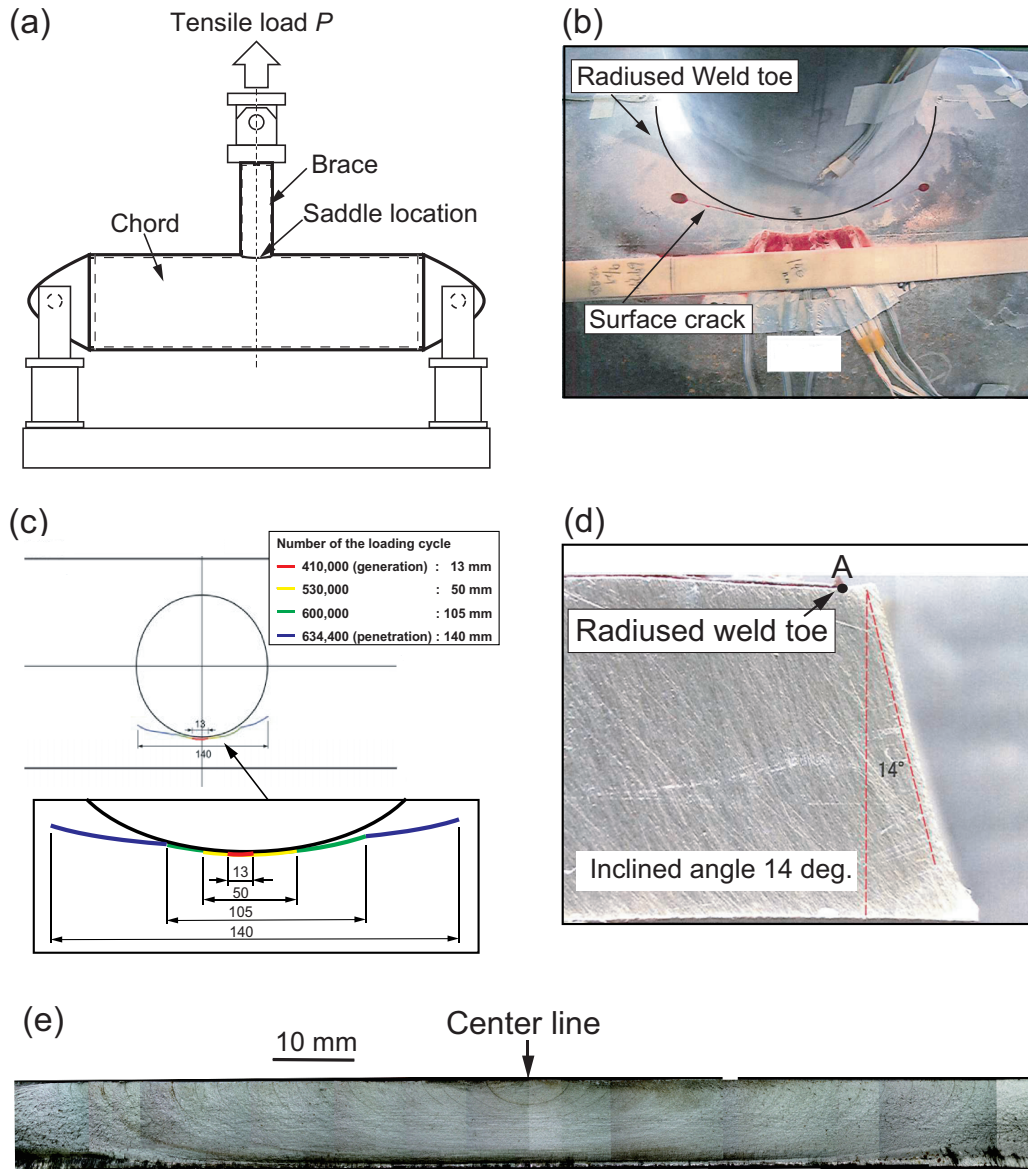


**Fig. 7.** Experimental results: (a) Overall view of the fatigue testing, (b) Crack propagation behavior, (c) Observation record of the crack trajectory, (d) Cross-section of fracture specimen, (e) Beach mark on the fracture surface.



the brace. A number of strain gauges were placed to quantitatively examine the stress distribution around the brace-chord intersection. Normal stress at the surfaces in their tangential direction was examined. Fatigue testing was performed subsequently: A cyclic load with a constant amplitude was applied to the top of the brace. The maximum tensile load was  $P_{cyclic}=140$  KN and the stress ratio was  $R=0.05$ . Under the cyclic loading, a propagating surface crack was generated at the saddle on the south part of the specimen. Its propagation was observed visually, and the shape of the surface crack was monitored with a beach mark technique. The air pressure inside the test specimen was kept at 1.1 atm and monitored during the fatigue test to check the penetration of the crack.

The crack propagation in the chord surface was visualized by means of dye penetrant inspection. Its trajectory is shown in Fig.7b. A major crack can be seen on the chord surface in the vicinity of the weld. The observation records of the crack propagation are presented in Fig.7c. A surface crack was found visually at the saddle with a width of 13 mm at about  $N=410,000$  cycles. The crack initially grew along the weld toe and reached a width of 50 mm at  $N=530,000$  cycles, while the mouth gradually extended from the weld toe. The width was 105 mm at  $N=600,000$  cycles. Finally, the surface crack penetrated the chord wall at  $N=634,400$  cycles. At this stage, its width was approximately 140 mm. To examine the inclination of the crack with respect to the chord thickness direction, the specimen was cut out at the saddle location. The cross-section of the fracture surface is shown in Fig.7d. The crack had a curvature toward the thickness direction with inclination of around 14 degree. The result from the beach mark test is shown in Fig.7e. A surface crack was generated from the saddle location and grew almost symmetrically with respect to the center line. Its ultimate shape was a semi-ellipse.

## 4. Numerical analysis of the test specimen

### 4.1. Stress evaluations of an intact tubular joint specimen

Before simulating the fracture behaviors of the tubular T-joint, a stress analysis was performed to examine the local stress around the weld. The numerical results were compared with the experimental results. The joint was modeled using 3D-CAD, and the quadratic tetrahedral FEs were generated automatically with the mesh generation system. The FE model is shown in Fig.8a. Global coordinates ( $x, y, z$ ) were defined. The  $y$ - and

$z$ -directions correspond to the longitudinal brace and chord directions, respectively. An FE model of a half-sized tubular joint was generated and symmetric boundary conditions were imposed. Both sides of the FE model were fixed. A uniaxial tensile load  $P_{static}=70$  KN was applied to the top of the brace. Fig.8b illustrates  $x$ - $y$  cross-section of the model at the saddle location. To generate a precise FE model including the weld toe geometry, the CAD data were modified to obtain a curvature radius  $\rho=11$  mm. The radiused weld toe (position A) is also shown. The whole structure was divided into a 8 mm mesh, and a 0.5 mm fine mesh was employed around the weld to obtain the stress distributions along the chord surface to high accuracy. The FE meshing at the weld is presented in Fig.8c. The FE model had about 653,400 nodes and 383,700 elements. Young's modulus was  $E=206$  GPa, and Poisson's ratio was  $\nu=0.3$ . Linear elastic analysis was performed. Residual stress was not considered in the numerical simulation.

The stress distribution around the weld was examined both numerically and experimentally. The location of the strain gauges is illustrated in Fig.8d. The stress distributions in the chord and brace surfaces were evaluated in three directions, *i.e.*, lines A, B and C, as shown in Figs.8c and d. The normal stress at the brace-chord surfaces in the tangential direction was measured along lines A and B from the radiused weld toe. The normal stress 4 mm from the weld toe (line C) was measured simultaneously. These results were compared with the maximum principal stress calculated by the FEM.

Fig.9a shows the stress distributions along lines A and B. The dashed lines with open marks are the surface stress evaluated with the measured strains, and solid lines with solid marks are the principal stress evaluated by the FEM. The single axis strain gauges were placed along maximum principal stress direction, and the surface stresses were evaluated based on the strains. The origins of lines A and B are the radiused weld toe as shown in Fig.8d. The surface stresses of the brace-chord intersection increased toward the weld. The stress on the chord surface was higher than that on the brace surface. The measured and calculated stress distributions along line A agree well, although some discrepancies can be seen near the weld toe. This may be attributable to the location of the strain gauges, which was 3 mm from the weld toe but could not be determined exactly because of the grinding. On the other hand, good agreement is observed between the measured and calculated stress distributions along line B. To further examine the local stress near the weld, the measured and calculated stress distributions along line C are compared in Fig.9b. The dashed and solid lines are measured

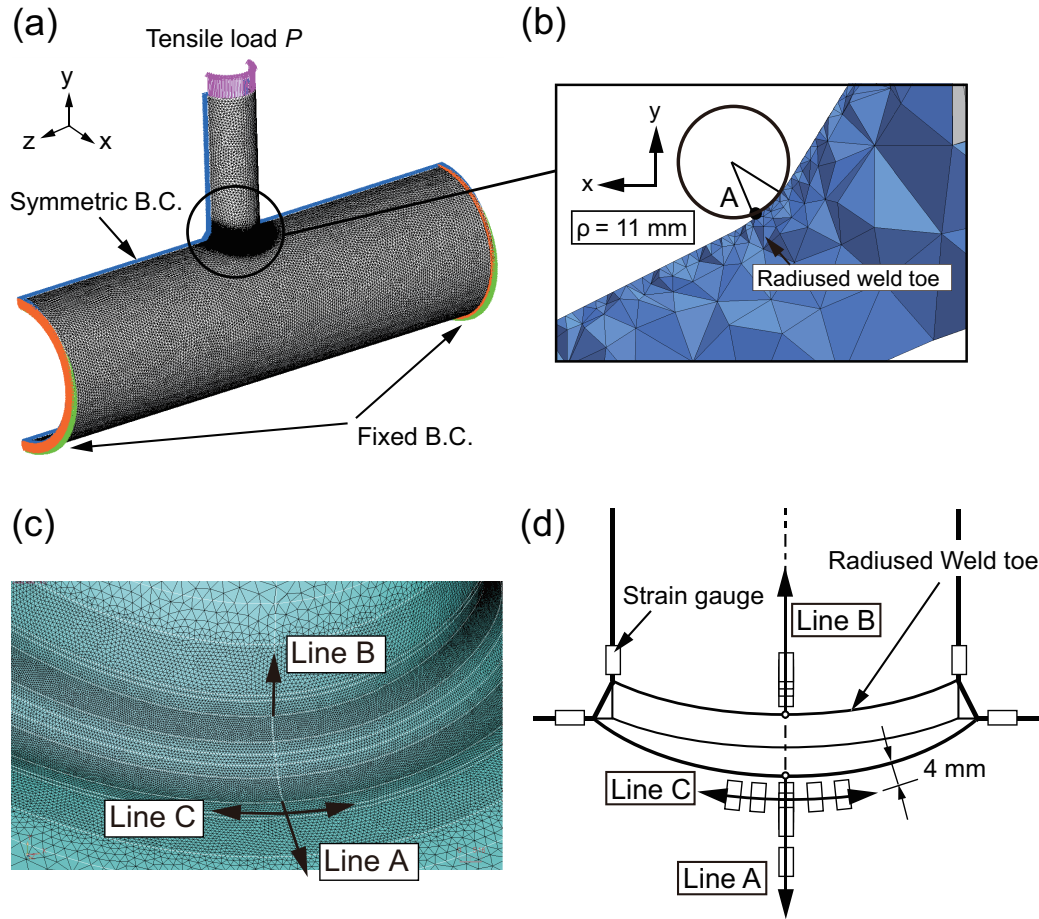


**Fig. 8.** FEM model of an un-cracked tubular T-joint: (a) FEM model, (b)  $x$ - $y$  cross-section of the saddle location, (c) FE meshing at the weld part and stress evaluation lines A, B and C, (d) Location of the strain gauges.

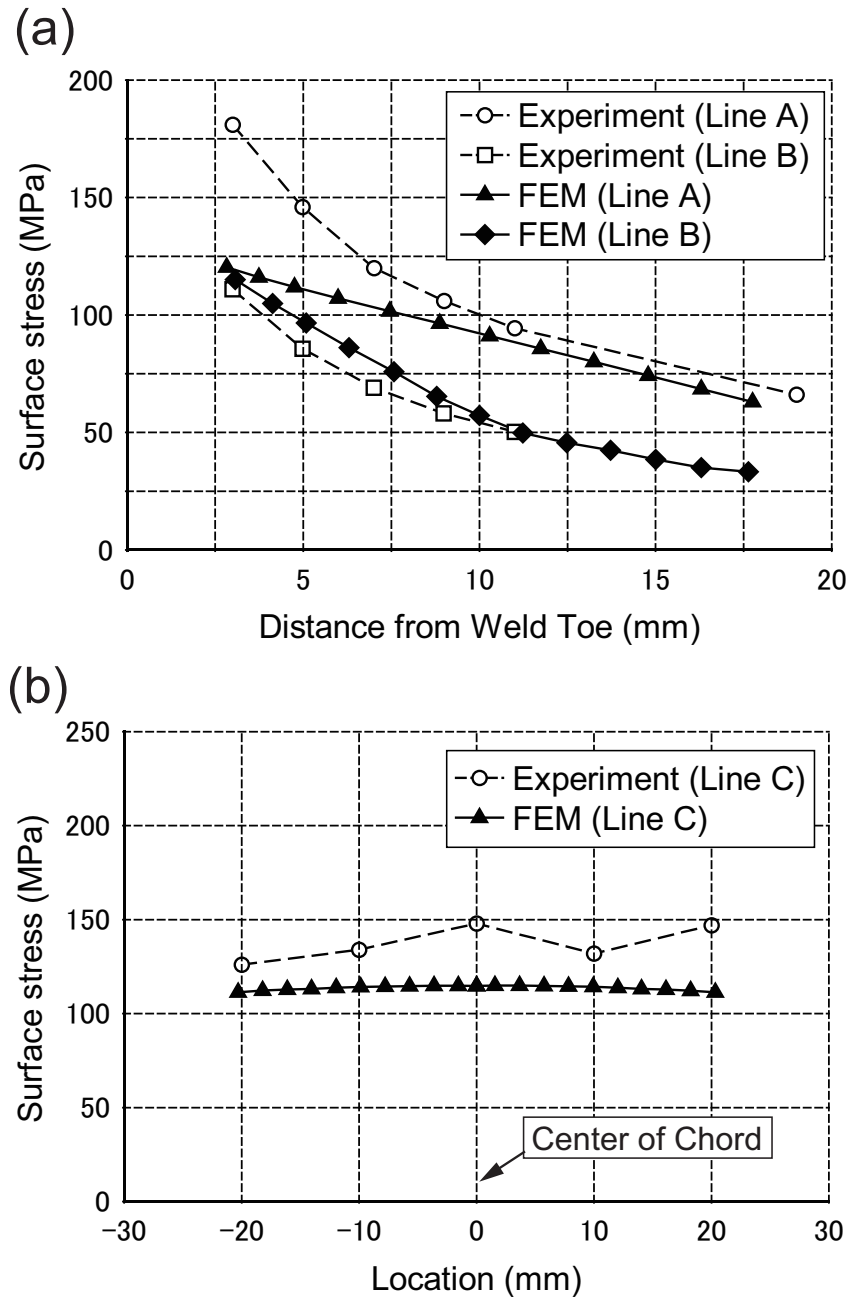


**Fig. 9.** Stress distribution near the weld toe: (a) Lines A and B, (c) Line C.

and calculated results, respectively. Although the measured stress is a little higher than the calculated stress, both exhibit nearly uniform distributions. Consequently, it can be concluded that the FEM modeling system proposed in this paper is effective for evaluating local stress in the joints of tubular structures.

#### 4.2. Crack propagation simulation in the tubular T-joint

Simulation of the crack propagation was performed based on the FEM model described in the previous section. It is known that the initial crack is generated in regions of stress concentration. Because the shape of the weld toe is complicated, the surface stresses were carefully examined in the region around the weld toe, where high stress concentration occurs. The maximum principal stress distribution along lines A and D of Fig.10a is shown in Fig.10b. The maximum stress can be observed around 3 mm from the radiused weld toe (position A). The initiation of the crack can be found in almost same position in the experiment, as shown in Fig.7d. An initial crack was thus inserted at this location in the FEM model to evaluate its propagation.

An overview of the cracked tubular joint and an initial crack placed on the saddle location is presented in Fig.11. The initial crack size can be defined by operators in the pre-processing step. A very small semi-circular surface crack ( $2c_0=0.4$  mm wide and  $a_0=0.2$  mm deep) was assumed, to simulate transient growth from a very small crack. The crack was inserted perpendicularly to the chord surface. A cyclic load  $\Delta P=133$  KN was applied with the stress ratio  $R=0.05$ . The overall structure was divided using a 5 mm mesh and the crack region, including the crack front, was divided using a very fine 0.05 mm mesh. There were 1,179,500 nodes and 752,300 elements in the initial model. Because the material data  $C$  and  $m$  for the fatigue testing were not available, from the Japan Society of Steel Construction (JSSC) [57] were respectively employed.  $C$  and  $m$  were evaluated by mean+2SD (Standard Deviation) curve. The data were obtained by performing regression analysis on fatigue crack propagation test results for steel welded joints carried out by the National Institute for Materials Science (NIMS), Japan [58]. The modified version of Paris' law in Eq.(5) was adopted. The coefficients were  $C=2.66704\text{e-}11$  (unit:m/cycle) and  $m=2.75$  and the threshold SIF was  $\Delta K_{th}=1.99223$  (unit:MPa $\sqrt{m}$ ). Nine-pass welding was used to fabricate the tubular joint. The welding heat input for these joints was comparable to the largest one in the NIMS database, and this leads to a faster propagation rate.

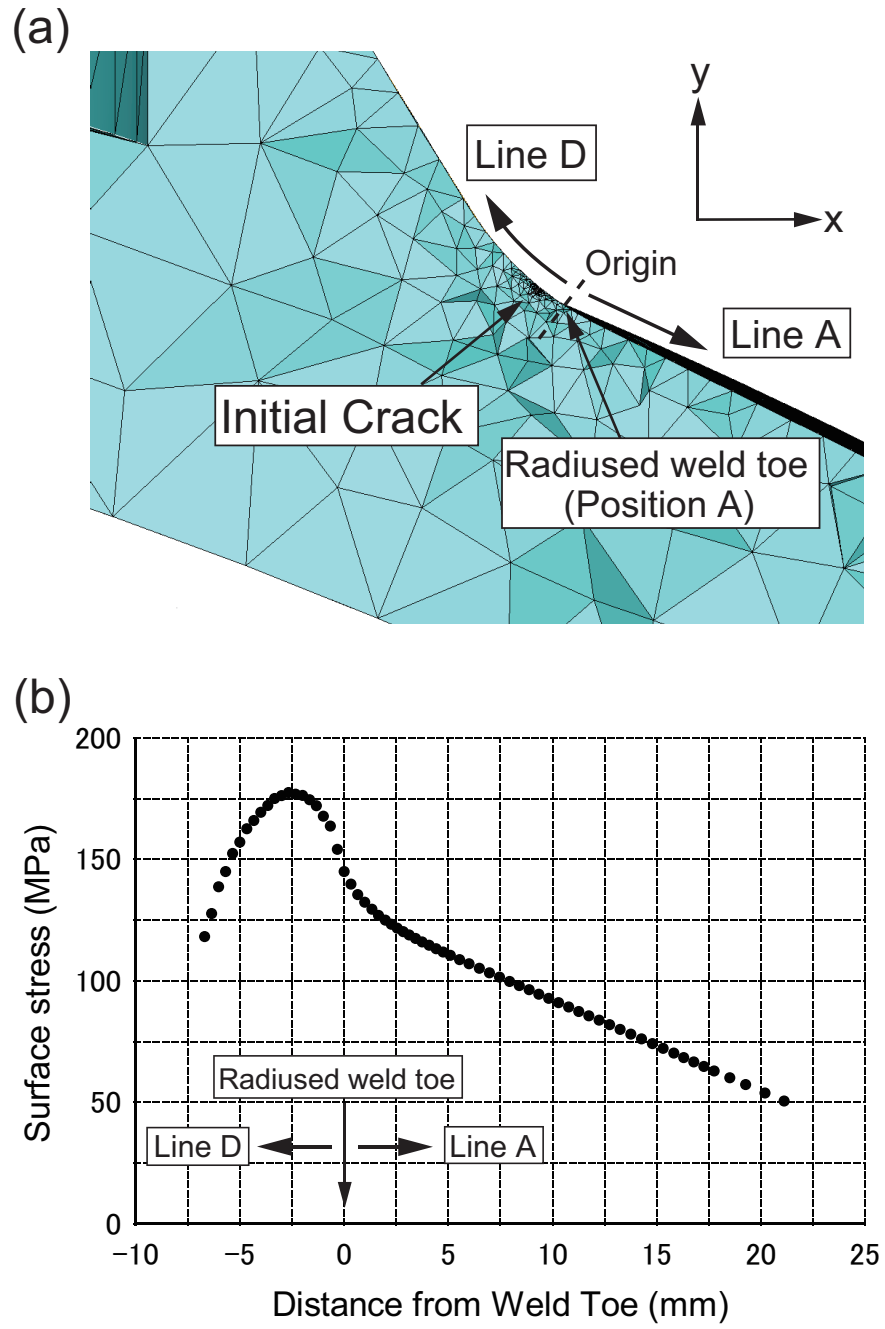


**Fig. 10.** Stress distribution at the saddle location: (a)  $x$ - $y$  cross-section of the FEM model at the saddle, (b) Stress distribution from the chord to weld surface.

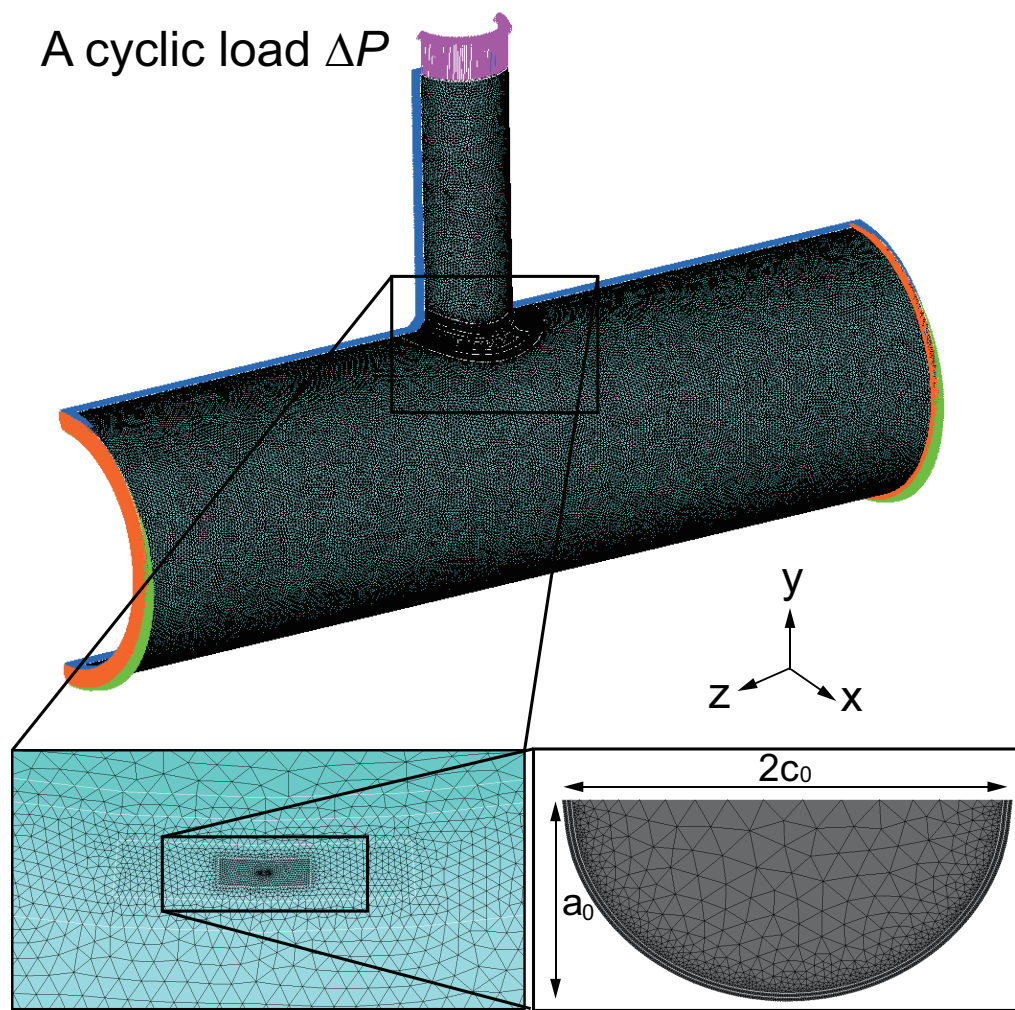


**Fig. 11.** A cracked tubular T-joint FEM model and details around the surface crack.

Therefore, the mean+2SD growth law was adopted. Simulation of the crack propagation was performed until the crack penetrated the chord wall.

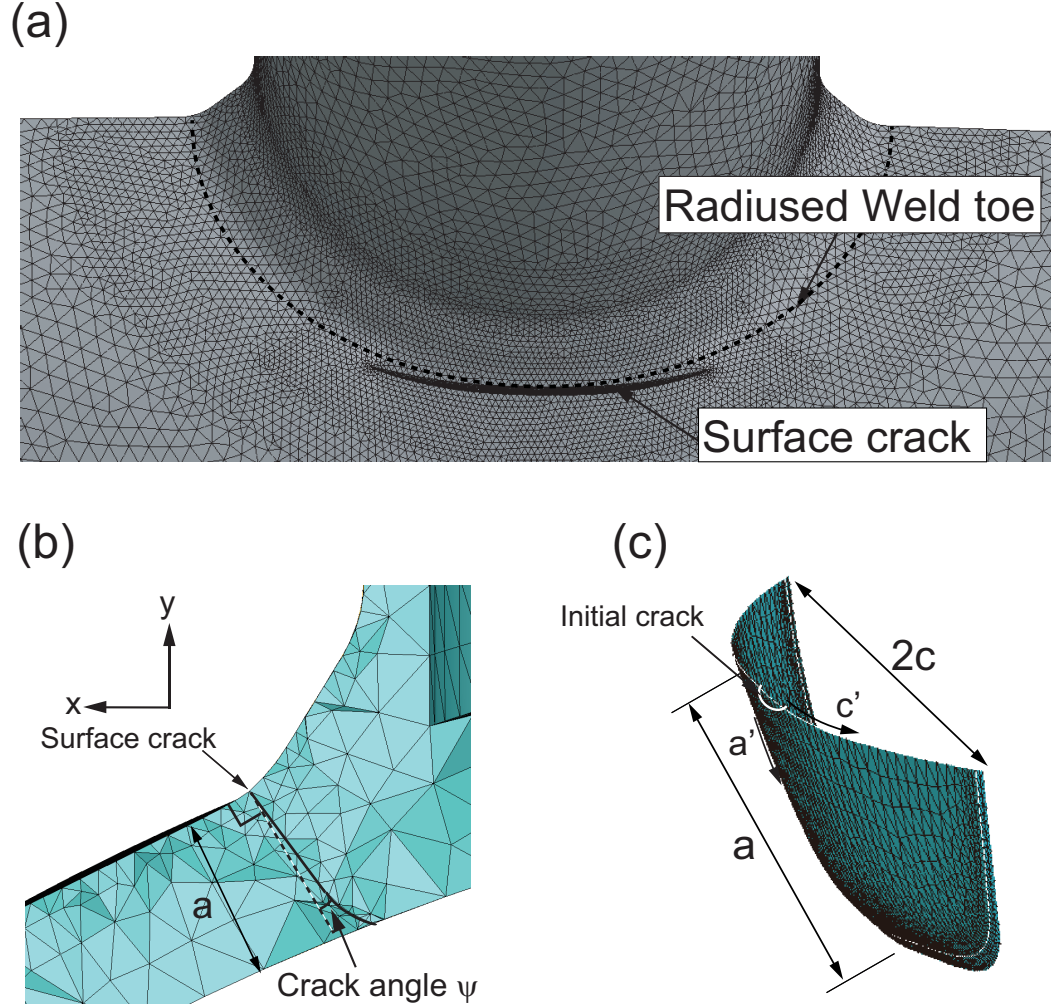


**Fig. 12.** Crack propagation simulation of the T-shaped tubular joint: (a) A surface crack at saddle location, (b)  $x$ - $y$  cross-section of the saddle location, (c) A doubly-curved surface crack.

In the simulation, the crack extension,  $\Delta_i$ , was fixed. Iteration of 168 steps was carried out, and there were  $N=325,200$  cycles in total. The numerical results are shown in Fig.12a. Initially, the crack front location at the free surface was curved along the weld because of the high stress con-



centration. The surface crack then grows apart from the weld toe. These phenomena were also observed in the experimental results as shown in Fig.6b. The FEM model cross-section from the saddle part in the  $x-y$  plane is shown in Fig.12b. The surface crack had a curvature toward the thickness direction of the chord. The doubly-curved surface crack form as shown in Fig.12c. The ultimate width and depth of the chord were  $2c=83.1$  mm and  $a=12.7$  mm, respectively.

## 5. Results and discussion

The fracture behaviors observed in the experimental results were studied by comparing the measured results with the calculations based on the fracture mechanics approach. Two behaviors are examined. One is the shape of the doubly-curved surface crack, and the other is a comparison of fatigue life between the numerical and experimental results. To examine the former, a very small crack was assumed at the weld toe in the computation. The fatigue life is compared with the numerical results using dye penetrant inspection and beach mark techniques.

### 5.1. Curvature of the developed surface crack

The curvature of the developed surface crack was examined first. The SIFs calculated at the crack front location at the free surface and at the deepest point are shown in Figs.13a and b, respectively. The local coordinates of the crack,  $a'$  and  $c'$ , along the arc of the surface crack are chosen as in Fig.12c. The horizontal axis of Fig.13a represents the width of the crack growth  $c'$  mm, and that of Fig.13b represents the depth  $a'$  mm indicated in Fig.12c. The vertical axis represents the SIFs. The evaluated SIFs vary smoothly as the crack grows.  $K_I$  at the crack front location at the free surface increases uniformly as the surface crack extend. At its deepest point,  $K_I$ , also increased until the surface crack reached half the length of the chord wall, after which it remained nearly constant. This is typical behavior when the propagation of a surface crack subjected to a bending load is observed. At both the crack front location at the free surface and the deepest point,  $K_{II}$  remains small compared with  $K_I$ ;  $K_{II}$  gradually increases and decreases at the mouth and the deepest point, respectively. The surface crack thus grew in the circumferential direction and down into the chord thickness, forming a doubly-curved surface, as shown in Fig.12c. Although the  $K_{III}$  was taken into account when the equivalent SIF was evaluated using Eq.(6), its effect

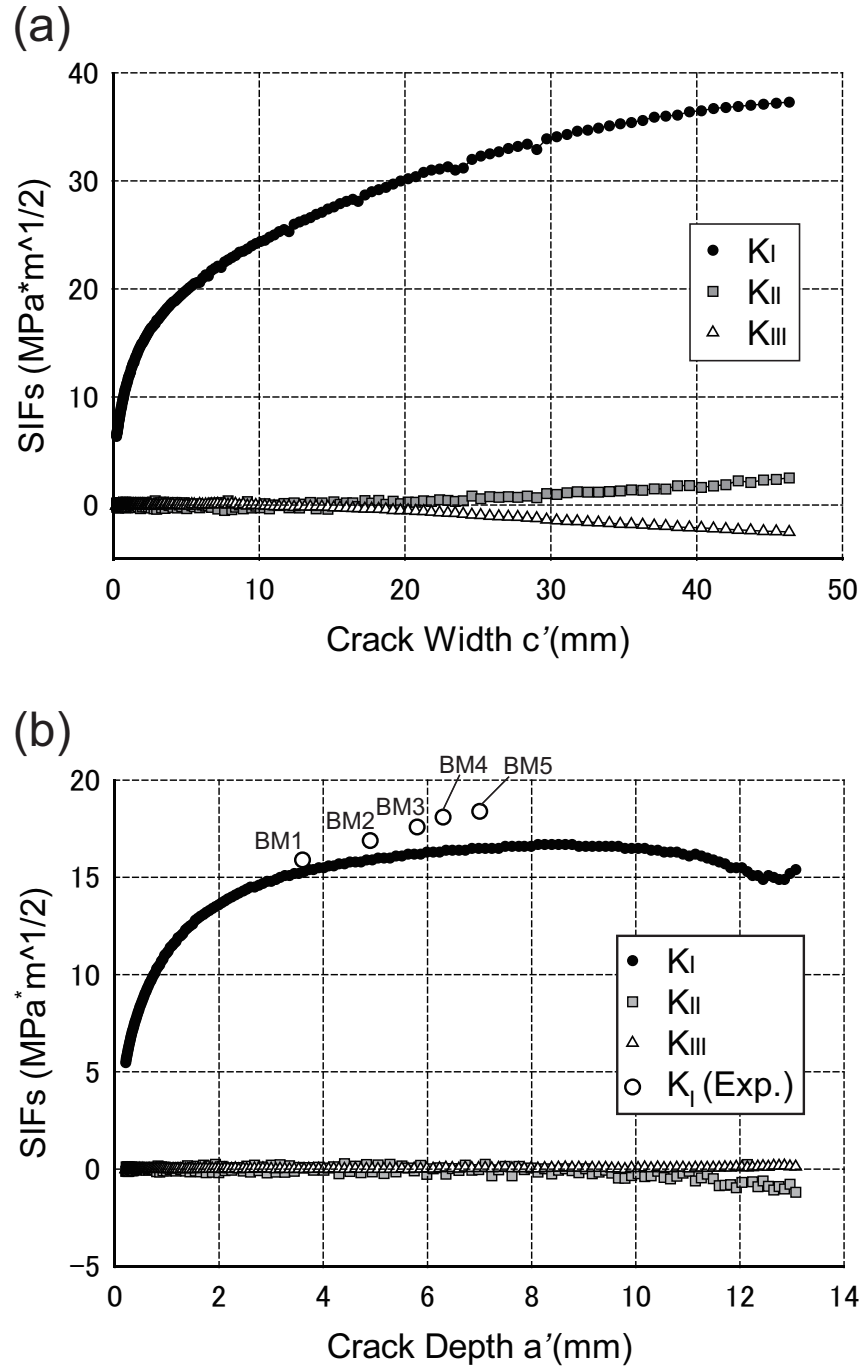


**Fig. 13.** The variations in the SIFs along the crack: (a) At crack front location at the free surface, (b) At deepest point.

was small. The crack propagation behavior simulated by the FEM analysis was in good agreement with the experimental results, as shown in Figs.7b and c.

The curvature of the surface crack toward the chord thickness direction was examined. The surface crack is curved as shown in Fig.12b. The crack angle  $\psi$  perpendicular to the chord surface was evaluated at the deepest point of the surface crack. The calculated result is presented in Fig.14. The experimental result is also presented in Fig.7d. The angle  $\psi$  in the calculated result is about 10 degrees. When the surface crack was small, the crack grew straight until it reached a half-thickness of the chord wall. The crack growth rate then gradually increased before the crack penetrated the chord wall. Consequently, the developed surface crack was curved at the deepest point. Similar phenomena were also observed in the experiment in Fig.7.

By employing FE modeling and the simulation system for 3D crack propagation, the process to generate a surface crack in a T-shaped tubular joint has been established, *i.e.*, a small planar surface defect propagates and forms a surface crack with a doubly-curved geometry. The mixed-mode surface crack develops under a complex stress distribution in the brace-chord intersection, and the mixed-mode state strongly influences generation of the doubly-curved surface. It has been reported in, *e.g.*, [4] that simulation of crack growth can be achieved with tetrahedral FE modeling and an automated mesh generation system through comparison of measured and calculated results.

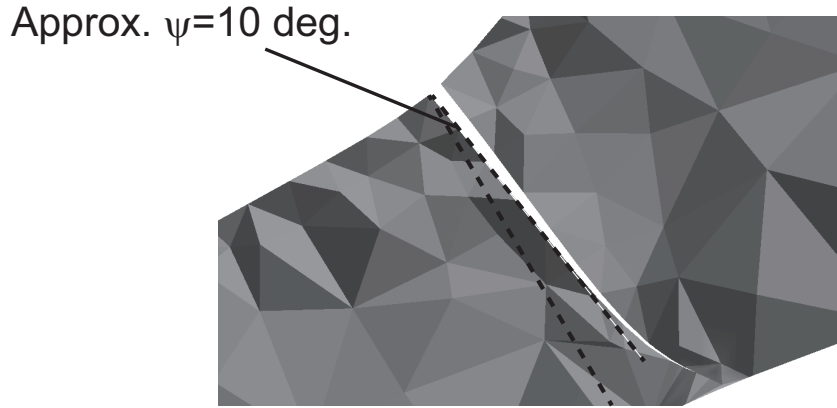


**Fig. 14.** Cross-section of the fracture surface at saddle location.

### 5.2. Crack propagation behavior

The propagation of the crack was examined by comparing the calculated and measured results. The developed surface crack had a doubly-curved shape. The fatigue life was compared with the numerical results using with dye penetrant inspection and beach mark techniques. The shape of this crack was mapped on to the plane of the initial surface crack, and the width and depth were measured. The results of beach mark testing are presented in Fig.15a. The solid line was the measured results and the dashed line was interpolated between the measured beach marks. The calculated results are shown in Fig.15b. The surface crack developed in a semi-elliptical shape because the bending load was dominant on the crack in the case. The SIFs are evaluated based on the actual crack size obtained by the experiment. The surface cracks of BM1 to BM5 in Fig.15a are respectively inserted in the FEM model, and SIFs are examined. It is noted that the surface cracks are assumed planar semi-elliptical shape and inserted at the radiused weld toe to the perpendicular the chord surface, for simplicity. The  $K_I$  at the deepest point is compared with the crack propagation results. The results are plotted in Fig.13b as BM1 to BM5, respectively. The  $K_I$  at the deepest point based on the actual crack depth is almost same with the simulation results. The aspect ratio of the developed crack is compared with the measured results in Fig.16, where  $T$  is the chord thickness. Because a semi-circular surface crack was assumed, the aspect ratio monotonically decreased as the crack extended. The crack width observed in the experiment is larger than that from the calculated results. This is because the material parameters  $C$  and  $m$  of the test specimen were not available and welding residual stress was not considered in the numerical simulation. However, the trends of the calculated and measured crack propagation behaviors coincide well.

The calculated and measured relationships between the size of the surface crack and the number of fatigue cycles were also compared. Because crack initiation cannot be simulated using our present system, the initial size was assumed based on the observation of the initial visible crack in the experiment. A surface crack was found at  $N=410,000$  cycles, of width was  $2c_{\text{exp}}=12.2$  mm, as shown in Fig.15a. Almost the same crack width was found at  $N=168,000$  cycles in the calculation, which was  $2c'_{\text{FEM}}=12.2$  mm, as shown in Fig.15b. For a comparison, the crack propagation simulation was carried out by employing the material data for BS7901 [59]. The coefficients were  $C=1.64755\text{e-}11$  (unit:m/cycle) and  $m=3$  and the threshold SIF was  $\Delta K_{th}=1.99223$  (unit:MPa $\sqrt{\text{m}}$ ). Paris' law of Eq.(4) was adopted to

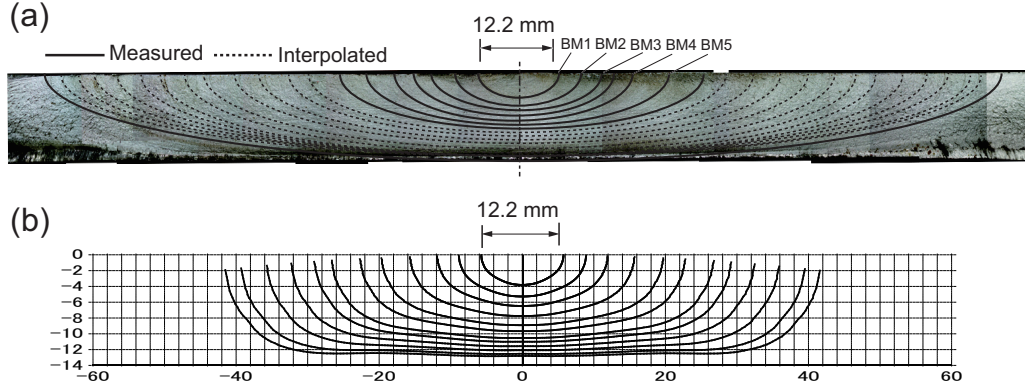


**Fig. 15.** Crack path: (a) Beach mark obtained by the experiment, (b) Crack path evaluated by the simulation.

evaluate the growth rate. The calculated and measured fatigue cycles were compared with each other starting from this surface crack sizes. The numerical results are shown in Fig.17. The simulation results with JSSC and BS7901 data are consistent. The measured behavior of the crack propagation was well simulated by calculation, as was curvature of the doubly-curved surface. Therefore, we confirm that the proposed system is effective in simulating the propagation of a surface crack in the joints of tubular structures. The material data  $C$  and  $m$  used in the crack propagation simulation were conservative, and the experimental and simulation results used almost the same number of cycles to penetrate the thickness. We assumed that if high heat input was introduced in the welding operation and heat treatment was not carried out after the welding procedure, the welding residual stress was strongly affected the experimental results.

Simulation of the propagation of a surface crack in a tubular T-joint was performed by employing the tetrahedral FE modeling and remeshing procedure with an automated mesh generation system. The VCCM for tetrahedral FEs was employed to determine the SIFs. Based on the calculated SIFs, the crack growth rate and direction were calculated. The propagation behavior simulated with the calculated SIFs correlated well with that observed in the experiment. We confirmed that the proposed system to simulate propagation of a 3D crack is effective for analyzing crack propagation behavior. This numerical technique can be applied not only to cracked tubular joint structures but also to other types of welded steel structures.

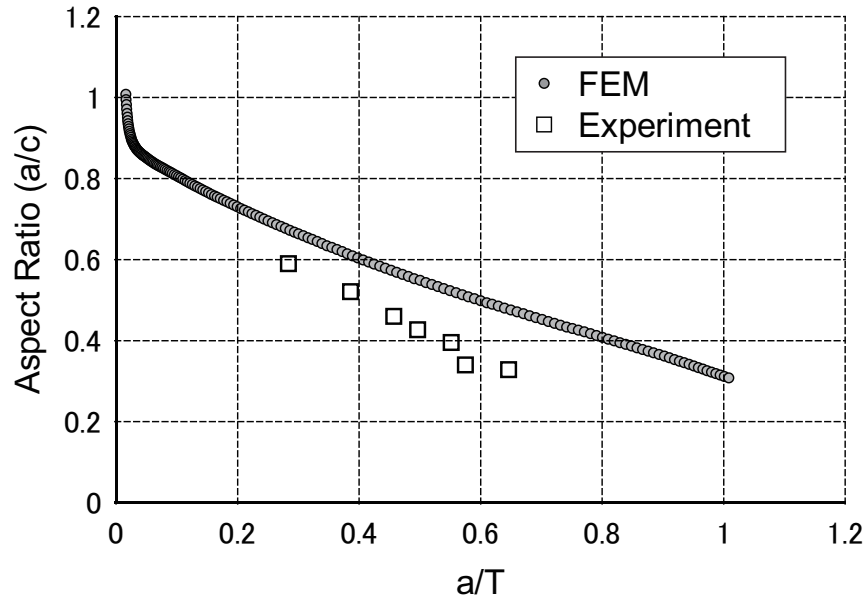


Fig. 16. Comparison of the aspect ratio  $a/c$  of the surface crack.

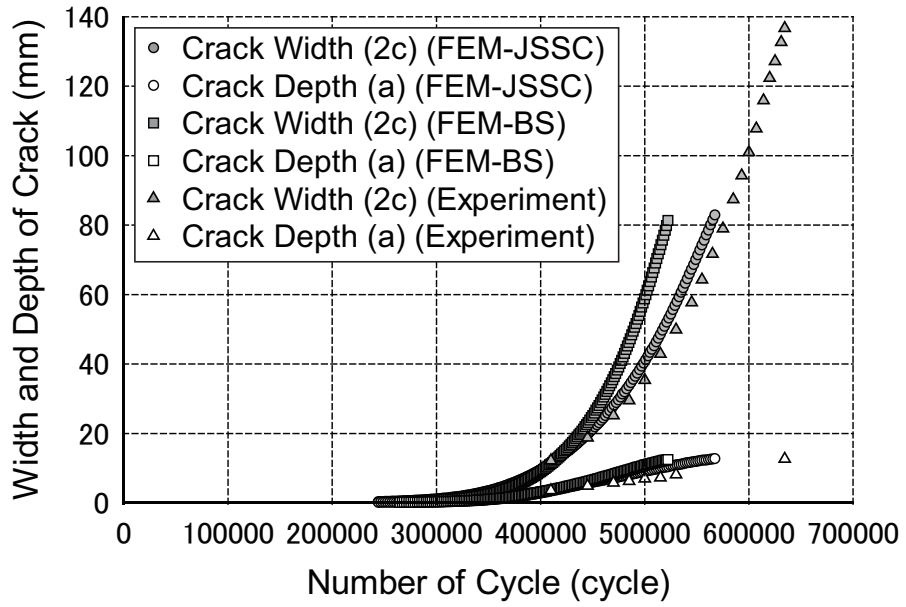


Fig. 17. Variation in crack width and depth for experimental and numerical results.

## 6. Conclusions

In this study, crack propagation behaviors in a tubular T-joint were examined by applying a newly developed software system to simulate crack propagation. A simulation system based on tetrahedral FE modeling was applied to the analysis of the crack growth in a tubular joint. The simulation procedures and SIFs evaluation techniques for quadratic tetrahedral FEs were described. In the fatigue test, two kinds of results were presented. One was surface stress under static load and the other was crack growth behavior under cyclic load. The numerical evaluations were carried out by the present system. The surface stresses were compared with the experimental results and the results are in good agreement. And, the crack initiation point is examined. The crack propagation simulation was carried out. The doubly-curved geometry of the developed surface crack was discussed by the SIFs. And, fatigue cycle was examined. These comparisons show that the simulation system to be effective in simulating crack propagation phenomena in the joints of tubular structures.

## Acknowledgements

This research was partially supported by the JSPS Grants-in-Aid for Young Scientists (B)(16K18323) and for Scientific Research (B)(15H04212) and (C)(15K06632). This work was performed as part of the Cooperative Research Program of the Joining and Welding Research Institute, Osaka University. I would like to express my gratitude to Mr. Takaaki Takei (Graduate School of Engineering, Hiroshima University) for giving us valuable comments on this research.

## References

- [1] Etube LS. Fatigue and fracture mechanics of offshore structures, Engineering Research Series. Professional Engineering Publishing, 2001.
- [2] Maddox SJ. Fatigue strength of welded structures, 2nd *ed.*. Woodhead Publishing, 2002.
- [3] Fricke W. Fatigue analysis of welded joints: state of development. Mar Struct 2003;16:185-200.

- [4] Bowness D, Lee MMK. Fatigue crack curvature under the weld toe in an offshore tubular joint. *Int J Fatig* 1998;20:481-90.
- [5] Bowness D, Lee MMK. The development of an accurate model for the fatigue assessment of doubly curved cracks in tubular joints. *Int J Fract* 1995;73:129-47.
- [6] Lee MMK. Strength, stress and fracture analyses of offshore tubular joints using finite elements. *J Const Steel Res* 1999;51:265-86.
- [7] Cao JJ, Yang GJ, Packer JA, Burdekin FM. Crack modeling in FE analysis of circular tubular joints. *Eng Fract Mech* 1998;61:537-53.
- [8] Chiew SP, Lie ST, Lee CK, Huang ZW. Stress intensity factors for a surface crack in a tubular T-joint. *Int J Pres Ves Pip* 2001;78:677-85.
- [9] Kam JCP, Dover WD, Ma CN. The prediction of crack shape development for in-service cracks in offshore welded tubular joints. *Mar Struct* 1995;8:37-65.
- [10] Bowness D, Lee MMK. Fracture mechanics assessment of fatigue cracks in offshore tubular structures. OTO Report 2000/077, Health and Safety Executive, 2002.
- [11] Borges L, Chiew S, Nussbaumer A, Lee C. Advanced numerical modeling of cracked tubular K joints: BEM and FEM Comparison. *J Bridge Eng* 2012;17:432-42.
- [12] Chang E, Dover WD. Weight function and stress intensity factor for a semi-elliptical surface saddle crack in a tubular welded joint. *J Strain Anal Eng* 2005;40:301-26.
- [13] Lee CK, Chiew SP, Lie ST, Nguyen TBN. Adaptive mesh generation procedures for thin-walled tubular structures. *Finite Elem Anal Des* 2010;46:114-31.
- [14] Qian X, Nguyen CT, Petchdemanengam Y, Ou Z, Swaddiwudhipong S, Marshall P. Fatigue performance of tubular X-joints with PJP+welds: II-Numerical investigation. *J Constr Steel Res* 2013;89:252-61.



- [15] Fleming M, Chu YA, Moran B, Belytschko T. Enriched element-free Galerkin methods for crack tip fields. *Int J Numer Meth Eng* 1997;40:1483-504.
- [16] Cisilino AP, Aliabadi MH. Three-dimensional BEM analysis for fatigue crack growth in welded components. *Int J Pres Ves Pip* 1997;70:135-44.
- [17] Belytschko T, Black T. Elastic crack growth in finite elements with minimal remeshing. *Int J Numer Meth Eng* 1999;45:601-20.
- [18] Nishioka T, Tokudome H, Kinoshita M. Dynamic fracture-path prediction in impact fracture phenomena using moving finite element method based on Delaunay automatic mesh generation. *Int J Solid Struct* 2001;38:5273-301.
- [19] Tanaka S, Okada H, Okazawa S, Fujikubo M. Fracture mechanics analyses using the wavelet Galerkin method and extended finite element method. *Int J Numer Meth Eng* 2013;93:1082-108.
- [20] Kikuchi M, Wada Y, Shintaku Y, Suga K, Li Y. Fatigue crack growth simulation in heterogeneous material using s-version FEM. *Int J Fatig* 2014;58:47-55.
- [21] Tanaka S, Suzuki H, Ueda S, Sannomaru S. An extended wavelet Galerkin method with a high-order B-spline for 2D crack problems. *Acta Mech* 2015;226:2159-75.
- [22] Tanaka S, Sannomaru S, Imachi M, Hagihara S, Okazawa S, Okada H. Analysis of dynamic stress concentration problems employing spline-based wavelet Galerkin method. *Eng Anal Bound Elem* 2015;58:129-39.
- [23] Tanaka S, Suzuki H, Sadamoto S, Imachi M, Bui QT. Analysis of cracked shear deformable plates by an effective meshfree plate formulation. *Eng Fract Mech* 2015;144:142-57.
- [24] Pang JHL, Tsang KS, Hoh HJ. 3D stress intensity factors for weld toe semi-elliptical surface cracks using XFEM. *Mar Struct* 2016;48:1-14.
- [25] Tanaka S, Suzuki H, Sadamoto S, Sannomaru S, Yu TT, Bui QT. J-integral evaluation for 2D mixed-mode crack problems employing a meshfree stabilized conforming nodal integration method. *Comput Mech* 2016;58:185-98.

- [26] Tanaka S, Suzuki H, Sadamot S, Okazawa S, Yu TT, Bui QT. Accurate evaluation of mixed-mode intensity factors of cracked shear-deformable plates by an enriched meshfree Galerkin formulation. *Arch Appl Mech* 10.1007/s00419-016-1193-x.
- [27] <http://adventure.sys.t.u-tokyo.ac.jp/> [accessed 16.03.31].
- [28] Lee CK, Tjhen LS, Ping CS, Yongbo S. Numerical models verification of cracked tubular T, Y and K-joints under combined loads. *Eng Fract Mech* 2005;72:983-1009.
- [29] Lie ST, Lee CK, Chiew SP, Shao YB. Validation of surface crack stress intensity factors of a tubular K-joint. *Int J Pres Ves Pip* 2005;82:610-7.
- [30] Qian X, Dodds Jr. RH, Choo YS. Mode mixity for tubular K-joints with weld toe cracks. *Eng Fract Mech* 2006;73:1321-42.
- [31] Rajaram H, Socrate S, Parks DM. Application of domain integral methods using tetrahedral elements to the determination of stress intensity factors. *Eng Fract Mech* 2000;66:455-82.
- [32] Nagai M, Ikeda T, Miyazaki N. Stress intensity factor analyses of three-dimensional interface cracks using tetrahedral finite elements. *Comput Mech* 2013;51:603-15.
- [33] Okada H, Kamibeppu T. A virtual crack closure-integral method (VCCM) for three-dimensional crack problems using linear tetrahedral finite elements. *Comput Model Eng Sci* 2005;10:229-38.
- [34] Okada H, Kawai H, Araki K. A virtual crack closure-integral method (VCCM) to compute the energy release rates and stress intensity factors based on quadratic tetrahedral finite elements. *Eng Fract Mech* 2008;75:4466-85.
- [35] Okada H, Ohata S. Three-dimensional J-integral evaluation for cracks with arbitrary curvatures and kinks based on domain integral method for quadratic tetrahedral finite element. *Eng Fract Mech* 2013;109:58-77.
- [36] Daimon R, Okada H. Mixed-mode stress intensity factor evaluation by interaction integral method for quadratic tetrahedral finite element with correction terms. *Eng Fract Mech* 2014;115:22-42.

- [37] Koshima T, Okada H. Three-dimensional J-integral evaluation for finite strain elastic-plastic solid using the quadratic tetrahedral finite element and automatic meshing methodology. *Eng Fract Mech* 2015;135:34-63.
- [38] Kaneko S, Okada H, Kawahi H. Development of Automated Crack Propagation Analysis System (Multiple Cracks and their Coalescence). *J Comput Sci Tech JSME* 2012;6:97-112.
- [39] Okada H, Kawai H, Tokuda T, Fukui Y. Fully automated mixed mode crack propagation analyses based on tetrahedral finite element and VCCM (virtual crack closure-integral method). *Int J Fatig* 2013;50:33-9.
- [40] Tanaka S, Okazawa S, Okada H, Xi Y, Ohtsuki Y. Analysis of three-dimensional surface crack in welded joint structure using shell-solid mixed method. *Int J Offshore Polar Eng* 2013;23:224-31.
- [41] Tanaka S, Kawahara T, Okada H. Study on crack propagation simulation of surface crack in welded joint structure. *Mar Struct* 2014;39:315-34.
- [42] Arai K, Yodo K, Okada H, Yamada T, Kawai H, Yoshimura S. Ultra-large scale fracture mechanics analysis using a parallel finite element method with submodel technique. *Finite Elem Anal Des* 2015;105:44-55.
- [43] <http://en.e-technostar.com/products/tsv-pre/> [accessed 16.03.31].
- [44] MSC.Nastran 2010. User's Guide.
- [45] Bažant ZP, Estenssoro LF. Surface singularity and crack propagation. *Int J Solid Struct* 1979;15:405-26.
- [46] Li Y, Hasegawa K, Katsumata G, Osakabe K, Okada H. Development of stress intensity factors for surface cracks with large aspect ratio in plates. *J Press Vess-T ASME* 2015;137:051207 1-8.
- [47] Qian J, Fatemi A. Mixed mode fatigue crack growth: A literature survey. *Eng Fract Mech* 1996;55:969-90.
- [48] Dell'Erba DN, Aliabadi MH. Three-dimensional thermo-mechanical fatigue crack growth using BEM. *Int J Fatig* 2000;22:261-73.

- [49] Schöllmann M, Fulland M, Richard HA. Development of a new software for adaptive crack growth simulations in 3D structures. *Eng Fract Mech* 2003;70:249-68.
- [50] Richard HA, Fulland M, Sander M. Theoretical crack path prediction. *Fatig Fract Eng Mater Struct* 2005;28:3-12.
- [51] Buchholz F-G, Chergui A, Richard HA. Fracture analysis and experimental results of crack growth under general mixed mode loading conditions. *Eng Fract Mech* 2004;71:455-68.
- [52] Paris P, Erdogan F. A critical analysis of crack propagation laws. *Trans ASME J Basic Eng* 1963;85:528-33.
- [53] Erdogan F, Sih GC. On the crack extension in plates under plane loading and transverse shear. *Trans ASME J Basic Eng* 1963;85:519-25.
- [54] Yagi K, Murakami T. Experimental study on fatigue life and crack propagation of tubular T-joint. *Conference Proceedings The JASNAOE* 2013;16:535-38. (in Japanese)
- [55] Yagi K, Murakami T. A Study on the relation between paint crack and steel crack of tubular T-joint. *Conference Proceedings The JASNAOE* 2013;17:93-6. (in Japanese)
- [56] Yagi K, Osawa N, Tanaka S, Kashima H. Comparative study on SN-based and FCP-based fatigue assessment techniques for T-shaped tubular welded joint. *Conference Proceedings of IIW* 2016:1-16 (XIII-2653-16).
- [57] Fatigue design recommendation for steel structures, Japanese Society of Steel Construction (JSSC), 2012. (in Japanese)
- [58] NIMS fatigue data sheet, No. 21, 31, 41, 46, 54, National Institute for Materials Science Japan, 1980-1986. (in Japanese)
- [59] BS 7910:2005. Guide to methods for assessing the acceptability of flaws in metallic structures British Standards Institution.